



Article

Into the Groove: A Multitechnique Insight into the DNA–Vemurafenib Interaction

Gabriele Cavalieri ¹, Riccardo Pison ¹, Domenico Marson ¹, Erik Laurini ^{1,*} and Sabrina Pricl ²

¹ Molecular Biology and Nanotechnology Laboratory (MolBNL@UniTS), DEA, University of Trieste, Piazzale Europa 1, 34127 Trieste, Italy; gabriele.cavalieri@phd.units.it (G.C.); riccardo.pison@studenti.units.it (R.P.); domenico.marson@dia.units.it (D.M.)

² Department of General Biophysics, Faculty of Biology and Environmental Protection, University of Lodz, ul. Pomorska 141/143, 90-236 Łódź, Poland; sabrina.pricl@dia.units.it

* Correspondence: erik.laurini@dia.units.it; Tel.: +39-040-5583432

Abstract: This study explores the interaction between Vemurafenib (VEM), a potent BRAF inhibitor, and calf thymus DNA (ctDNA) using a comprehensive array of biophysical and computational techniques. The primary objective is to understand the potential off-target effects of VEM on DNA, given its established role in melanoma therapy targeting the BRAF V600E mutation. The investigation employed methods such as ultraviolet–visible absorption spectroscopy, steady-state fluorescence, circular dichroism, isothermal titration calorimetry, and advanced molecular dynamics simulations. The results indicate that VEM interacts with DNA primarily through a minor groove-binding mechanism, causing minimal structural disruption to the DNA double helix. Viscosity measurements and melting temperature analyses further confirmed this non-intercalative mode of binding. Calorimetry data revealed an exothermic, thermodynamically favorable interaction between VEM and ctDNA, driven by both enthalpic and entropic factors. Finally, computer simulations identified the most probable binding site and mode of VEM within the minor groove of the nucleic acid, providing a molecular basis for the experimental findings.

Keywords: vemurafenib; calf thymus DNA; spectroscopic techniques; molecular simulations; binding affinity



Citation: Cavalieri, G.; Pison, R.; Marson, D.; Laurini, E.; Pricl, S. Into the Groove: A Multitechnique Insight into the DNA–Vemurafenib Interaction. *Appl. Biosci.* **2024**, *3*, 468–483. <https://doi.org/10.3390/applbiosci3040030>

Academic Editors: Francesco Cappello and Maria Grazia Palmerini

Received: 7 September 2024

Revised: 10 October 2024

Accepted: 15 October 2024

Published: 21 October 2024



Copyright: © 2024 by the authors. Licensee MDPI, Basel, Switzerland. This article is an open access article distributed under the terms and conditions of the Creative Commons Attribution (CC BY) license (<https://creativecommons.org/licenses/by/4.0/>).

1. Introduction

The binding of small molecules to nucleic acids (NAs) and DNA in particular represents a cornerstone of molecular biology, with profound implications for understanding gene regulation, drug design, and the development of novel therapeutic agents [1–3]. Small molecules can interact with DNA through a variety of modes, including intercalation, groove binding, electrostatic binding, and covalent attachment, each offering unique insights into the structural and functional nuances of the NA double helix [4,5]. These interactions are not only crucial in deciphering the fundamental principles of nucleic acid chemistry, but also serve as the foundation for the design of targeted pharmaceuticals, particularly in the realm of oncology [6,7] and antimicrobial therapy [8,9]. One such small molecule of significant interest is Vemurafenib (VEM) [10], a potent BRAF inhibitor that has revolutionized the therapeutic landscape for patients with metastatic melanoma, which harbors the BRAF V600E mutation. Its mechanism of action involves selective inhibition of the mutated BRAF kinase, thus disrupting the aberrant MAPK signaling pathway that drives tumorigenesis in this subset of melanomas. [11]. However, despite the fact that its primary mechanism of action is not directed at DNA, understanding its potential interactions with the NA is crucial for several reasons. First, the off-target effects of VEM on DNA could lead to unintended genotoxicity, which could manifest as secondary malignancies or other adverse effects. Second, it is essential to elucidate the nature of DNA–VEM interactions to ensure that they do not interfere with the normal biological processes of the NA, such

as replication, repair, and transcription, which are vital to maintaining genomic integrity. Therefore, studying the binding of VEM to DNA is not only a matter of understanding its primary pharmacological profile but also a necessary step in minimizing its side effects and optimizing its safety profile. The motivation behind this investigation lies in the need to fully characterize the molecular interactions of VEM, particularly in a clinical context where long-term administration could lead to cumulative off-target effects. By comprehensively assessing how VEM interacts with DNA, potential risks can be better predicted and mitigated, thus improving patient outcomes.

In order to explore the VEM–DNA interactions, in this work, a range of biophysical and biochemical techniques were employed. State-of-the-art spectroscopic methods, including ultraviolet–visible absorption (UV-vis), steady-state fluorescence (SSF), and circular dichroism (CD), along with viscosity measurements, were used to gain insight into the binding affinity, mode, and conformational changes induced by VEM binding to DNA. Isothermal titration calorimetry (ITC) was applied to measure the thermodynamic parameters of the binding interaction, providing quantitative data on binding enthalpy, entropy, and the overall affinity of VEM for DNA. Additionally, computational approaches, such as the On-the-Fly Probability Enhanced Sampling with METADynamics-like target distribution (OPES-METAD), and classical molecular dynamics simulations, were utilized to predict binding sites and elucidate the dynamic behavior of these complexes *in silico*. Together, these methodologies formed a comprehensive toolkit that allowed a detailed and nuanced understanding of the interactions between VEM and the NA.

2. Materials and Methods

2.1. Reagents and Chemicals

Rhodamine B (RhB), Acridine Orange (AO), calf thymus DNA (ctDNA), and all other reagents (analytical grade) were obtained from Sigma Aldrich Inc. (Saint Louis, MO, USA), while Vemurafenib was purchased from MedChemExpress (Monmouth, NJ, USA).

2.2. Sample Preparation and Analytical Procedures

Stock solutions of ctDNA, RhB, and AO were prepared by dissolving the appropriate amounts in 1× phosphate-buffered saline (PBS, pH = 7.4). These stock solutions were stored at 4 °C in the dark. The purity of ctDNA was confirmed by measuring the UV absorbance ratio ($A_{260}/A_{280} > 1.8$). The 10 mM stock solution of VEM was prepared in DMSO.

2.3. UV–Visible Absorption Spectroscopy

UV-vis absorption spectra were recorded at 25 °C using a V-730ST spectrophotometer (Jasco, Tokyo, Japan) equipped with a quartz cuvette (1.0 cm). To ensure complete interaction, each system was left to stand for 2 h. The UV spectra of a 50 μM ctDNA solution were acquired in the wavelength (λ) interval 225–350 nm before and after adding five incremental concentrations of VEM (from 5 to 100 μM), with the corresponding VEM solutions serving as references. Similarly, the UV spectra of a 50 μM VEM solution were measured in a range of 240 to 400 nm before and after the sequential addition of incremental ctDNA concentrations (from 5 to 100 μM). All experiments were carried out in triplicate.

2.3.1. DNA Melting Study

ctDNA melting studies were performed by measuring the absorption at $\lambda = 260$ nm of ctDNA (50 μM) in a temperature range of 25–100 °C, both in the absence and presence of equimolar concentrations of VEM, RhB, or AO. The temperature was increased at a rate of 1 °C/min. Data are presented as the fraction of single-stranded ctDNA (f_{ss}) as a function of temperature, where f_{ss} is expressed as $f_{ss} = (A - A_0)/(A_f - A_0)$. Here, A is the absorbance of the system at each experimental temperature, A_f is the absorbance at the final temperature (100 °C), and A_0 is the absorbance at the initial temperature (25 °C). The first

derivative of f_{ss} with respect to temperature was used for the numerical determination of the melting temperature T_m ($f_{ss} = 0.5$).

2.3.2. Effect of the Ionic Strength

The effect of ionic strength on the interaction between ctDNA and VEM was investigated by recording the absorbance ($\lambda = 260$ nm) at room temperature of mixed solutions containing ctDNA (50 μ M) and VEM (10 μ M) at different NaCl concentrations (0–0.1 M). Data are reported as mean values obtained from three independent measurements and represented as the normalized absorbance ratio A_0/A , where A_0 is the absorbance value for the ctDNA/VEM system in the absence of added salt and A is the absorbance of the system at each experimental NaCl concentration.

2.4. Viscosity Measurements

The room temperature viscosity of ctDNA (100 μ M) in the presence of VEM, RhB, and OA was assessed with an Ostwald viscometer. Temperature control was ensured by a thermostatically controlled water bath at different ligand–ctDNA molar ratios ([Ligand]/[ctDNA]). To ensure equilibrium binding, each mixture was left to stand for 30 min prior to measurement. The relative viscosity (η/η_0) of each sample was calculated by measuring the flow time of the solution through the viscometer (where η_0 represents the viscosity of ctDNA alone, and η is the viscosity of the ctDNA–ligand complex), and the data are presented as $(\eta/\eta_0)^{1/3}$ as a function of [ligand/ctDNA]. For each solution, the flow time was recorded in triplicate using a digital timer, and the average of these measurements was used to calculate the corresponding viscosity.

2.5. Circular Dichroism Spectroscopy

CD spectra were acquired between 220 and 320 nm at a scan speed of 20 nm/min and a temperature of 25 °C using a J-1500 spectropolarimeter (Jasco, Japan) fitted with a thermostatic cell holder and a PML-534 FD CD detector. A path length of 0.2 cm was used, with the spectral resolution parameters set to a step size of 0.5 nm and a bandwidth of 1 nm. In these experiments, the ctDNA concentration was fixed at 50 μ M, while the effects of VEM addition were tested at drug concentrations of 50 and 100 μ M. The spectral data were adjusted by subtracting the baseline derived from the pure buffer solution, and the final CD profiles represent the mean of three accumulations. All spectra were processed and analyzed using the Jasco Spectra Manager software (version 2.15.01, Jasco Corporation, Japan, 2020).

2.6. Steady-State Fluorescence Spectroscopy

The FP-8350 spectrofluorometer (Jasco, Japan), featuring a thermostatic cell holder and a 1 cm quartz cuvette, was employed for all SSF measurements. Fluorescence emission spectra were recorded using mixtures of ctDNA (50 μ M) with the fluorescent probe RhB (5 μ M) or AO (5 μ M), both in the presence and absence of variable concentrations of VEM (0–100 μ M). The excitation λ for RhB and AO was set at 465 nm and 495 nm, respectively, with the corresponding emission spectra recorded at 576 and 525 nm, respectively. All spectra were measured three times and are presented as average spectra.

2.7. Isothermal Titration Calorimetry Studies

The thermodynamics of the ctDNA–VEM complex formation was analyzed through ITC using a MicroCal PEAQ-ITC calorimeter (Malvern, UK) at 25, 30, 37, and 40 °C with a cell volume of 208 μ L. The sample cell contained a 40 μ M ctDNA solution in PBS, while the syringe was loaded with a 200 μ M VEM solution. Prior to the experiments, all solutions and the buffer were degassed for 30 min at each corresponding temperature. Titrations were performed in 19 sequential injections of 2 μ L, with constant stirring at 750 rpm. Control experiments were conducted to account for non-specific heats, and the resulting data were corrected by subtracting these values. The heat capacity (ΔC_p) was calculated from the

slope of the enthalpy versus temperature plot. Each experiment was performed in triplicate, and data acquisition and analysis were completed using GraphPad Prism 8.0.0 (GraphPad Software, San Diego, CA, USA).

2.8. Computer Simulations

Atomistic molecular dynamics (MD) simulations were used to gain a deeper insight into the interactions between the drug and the NA. As a representative of the ctDNA macromolecule, a 14-mer with the sequence 5'-CAACGTTGGCCAAC-3', already used in similar studies [12], was selected. The starting structure of this 14-mer was created with the *nab* (Nucleic Acid Builder) tool provided by AMBER22 [13] and parametrized with the OL15 AMBER forcefield [13]. The structure and parametrization of VEM were taken from our previous work [14]. Briefly, the parametrization relied on the gaff2 forcefield [15], with charges provided by the RESP ESP charge Derive server [16].

With no experimental information available on the interaction mode between VEM and the DNA molecule at hand, an enhanced MD method was employed, the On-the-Fly Probability Enhanced Sampling with METADynamics-like target distribution (OPES-METAD [17]) technique, provided by the PLUMED library [18]. Initially, the DNA–VEM complexes were manually constructed and solvated with TIP3P water molecules in a simulation box, maintaining a minimum distance of 24 Å from each solute atom. Sodium and chloride ions were added to the system to achieve a physiological salt concentration of 0.15 M NaCl. The solvated complexes then underwent energy minimization, which involved 5000 steps using the steepest descent method, followed by an additional 5000 steps of the conjugate gradient algorithm. The minimized structures were heated in the NVT (constant number of particles, temperature, and volume) ensemble for 100 ps from 0 to 300 K, with the Langevin thermostat [19] maintaining the temperature (collision frequency 2 ps^{-1}). The density of the systems was then equilibrated for 10 ns in the NPT (constant number of particles, temperature, and pressure) ensemble, applying the Berendsen barostat [20] ($P = 1 \text{ atm}$). From these simulations, the snapshots for the OPES-METAD simulations were extracted. Within the framework of OPES-METAD, a bias is added along selected collective variables (CVs) during the simulation (here, once every 1 ps, with an estimation of the maximum free energy barrier equal to 25 kcal/mol), allowing the system to quickly explore less energetically favorable states. The ensemble of configurations obtained can then easily be reweighted to obtain the unbiased ensemble. Two CVs were selected to drive the OPES-METAD simulations: a) the distance from the center of mass (COM) of VEM and the COM of the first base pair of the DNA molecule (dEDGE), and b) the number of contacts between DNA and VEM heavy atoms, calculated with the PLUMED COORDINATION function (parameters $r_0 = 6 \text{ Å}$, a and b equal to 6 and 12, respectively). Additionally, a restraint potential was applied to the latter CV ($k = 25 \text{ kcal/mol}$, acting when the number of contacts fell below 150), preventing exploration of states where the drug is not bound to the DNA molecule. The multiple-walkers variant of OPES-METAD was exploited, allowing 32 simulations starting from different VEM–DNA complexes to construct the biasing potential in parallel. Each simulation was carried out for 100 ns, totaling 3.2 μs of data collection. The simulation frames were reweighted to obtain the corresponding unbiased ensemble. At this point, two new sets of CVs were defined; the former set was defined as the minimum distance between the COM of VEM and the COM of any CG (dCG) or AT (dAT) base pair, and the latter set was formed by the two distances dEDGE and dCG. From the analysis of the corresponding free energy surfaces (FESs) obtained from the new CV sets, a well-defined binding site for VEM on the DNA molecule could be easily identified and extracted from the region at the lowest minima. The minimum energy structure was then subjected to a 4 μs unbiased MD simulation in the NPT ensemble (pressure maintained by the Monte Carlo barostat [21]), to collect all the data needed to describe the VEM–DNA interactions. In all MD simulations, the SHAKE algorithm [22] was applied to constrain all hydrogen atoms and the hydrogen mass repartitioning scheme [23] was used to enable a 4 fs time step. Electrostatic interactions were calculated using the particle mesh Ewald

(PME) method [24]. Unbiased MD simulations were performed with the GPU-accelerated pmemd module of AMBER22 [25], while the OPES-METAD simulations were carried out with GROMACS 2022.4 [26], patched with the PLUMED library [18] (version 2.9.1). All simulations were run on our hybrid GPU–CPU cluster, as well as on the pre-exascale Leonardo supercomputer (CINECA high-performance computing (HPC) infrastructure, Bologna, Italy). Trajectory analysis was carried out with the PYTRAJ module provided by AMBER22 [25], and in-house Python scripts.

3. Results and Discussion

3.1. UV–Visible Spectroscopy Assays

3.1.1. Absorption Spectra of the Interaction of Vemurafenib with ctDNA

The UV-vis absorption spectroscopy experiments undertaken in this study have yielded valuable insights into the interaction dynamics between VEM and DNA ctDNA. By examining the variations in absorbance relative to different concentrations of the drug or DNA, it was possible to elucidate the binding properties of VEM and assess its influence on the structural integrity of the NA. When the concentration of DNA was kept constant and the concentration of VEM gradually increased, the UV-vis absorption spectra displayed a moderate hyperchromic effect, as shown in Figure 1a. This increase in absorbance, particularly around the characteristic absorbance peaks of DNA at 260 nm, indicates changes in the electronic environment of the nucleobases. Hyperchromicity in DNA spectra typically suggests a perturbation in the base-stacking interactions within the double helix [27]. In the case of VEM, the moderate hyperchromic effect observed suggests that the drug interacts with the DNA in a manner that only slightly disturbs the stacking of the bases, without causing significant structural alterations to the overall helix. This type of spectral change is characteristic of small molecules that bind in the minor groove of DNA, where they induce local structural modifications without the extensive unwinding or lengthening of the helix associated with intercalation [28]. Importantly, this moderate hyperchromicity occurs in the absence of a bathochromic shift (redshift) in the absorbance maximum. A bathochromic shift would be expected if VEM intercalated between the base pairs, as intercalation typically leads to increased π - π stacking interactions between the drug and the nucleobases, resulting in a redshift. The lack of such a shift in the UV spectra reinforces the idea that VEM does not intercalate into the DNA but rather binds within the minor groove, affecting the electronic environment of the bases without significantly altering the helical pitch or base pair distance.

In a complementary set of experiments, the UV-vis absorbance of VEM was examined while the concentration of DNA was varied, keeping the drug concentration constant. In this scenario, a hypochromic effect was observed, where the absorbance of VEM decreased as more DNA was added to the solution, as shown in Figure 1b. Hypochromicity is a common indication of binding interactions in which the chromophore (in this case, VEM) experiences a decrease in electronic transition probabilities due to binding-induced conformational changes or the shielding effects of the DNA environment. The absence of a bathochromic shift in this setup further supports the hypothesis of groove binding. If VEM were intercalated into the DNA, one would expect not only a significant increase in absorbance (hyperchromicity), but also a notable shift in the wavelength of maximum absorbance due to the enhanced stacking interactions between the drug and the DNA bases. The fact that the absorbance decreases (hypochromicity) instead, without shifting, is indicative of VEM binding externally to the DNA helix, likely in the minor groove. In this binding mode, VEM likely interacts with the edges of the base pairs and the sugar-phosphate backbone, fitting snugly into the groove without disrupting the overall helical structure of the DNA. This mode of interaction is crucial as it suggests that VEM potentially does not induce significant genotoxic stress or compromise the integrity of the DNA double helix.

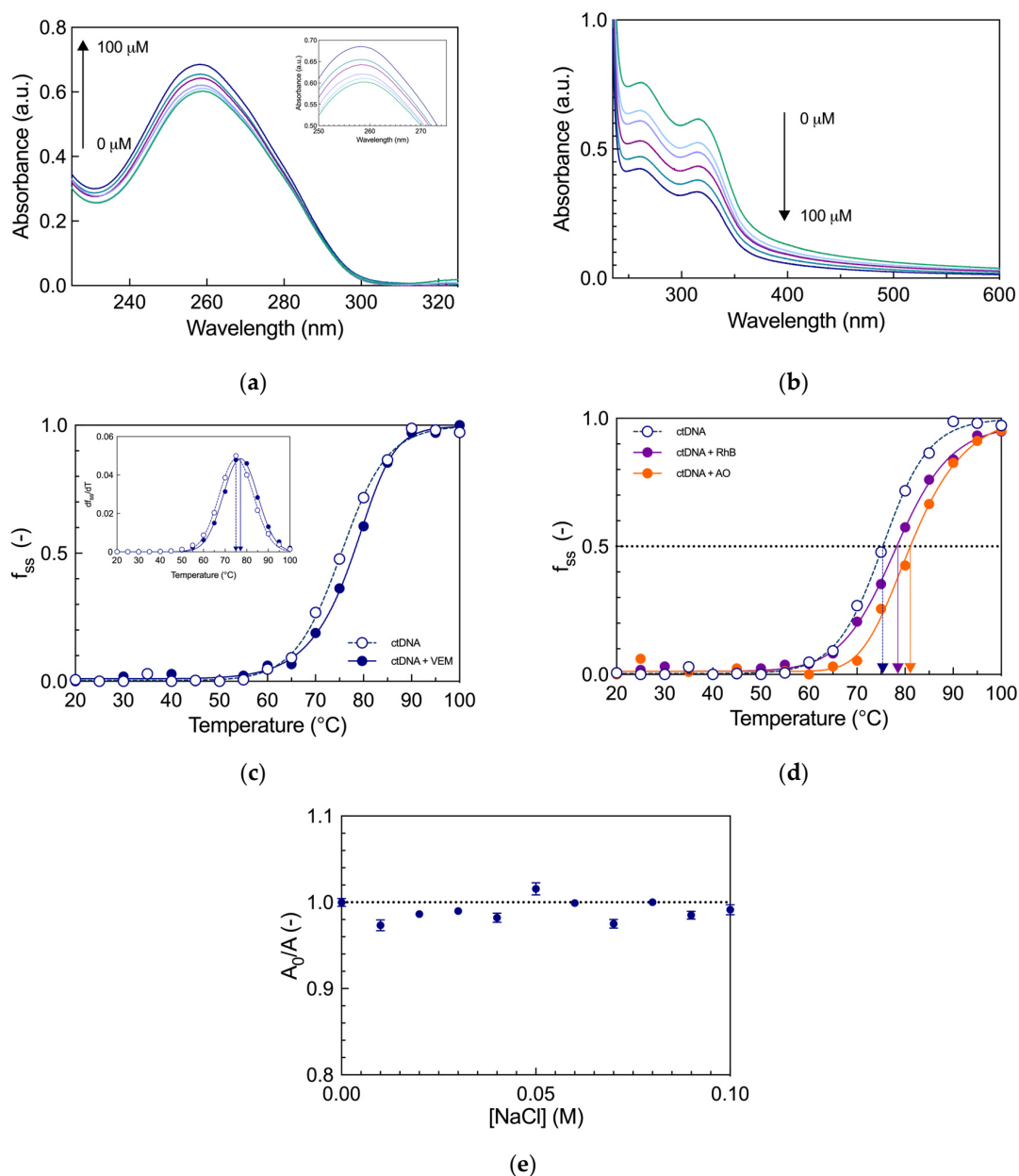


Figure 1. (a) UV-vis spectra of ctDNA (50 μM, green) before and after the addition of VEM (5 μM sky blue, 10 μM cornflower blue, 25 μM purple, 50 μM dark cyan and 100 μM navy blue) (PBS buffer, pH = 7.4, 25 °C). The inset shows a magnified view of the absorption region from 250 to 275 nm. (b) UV-vis spectra of VEM (50 μM, green) before and after the addition of ctDNA (5 μM sky blue, 10 μM cornflower blue, 25 μM purple, 50 μM dark cyan and 100 μM navy blue) under the same conditions. (c) Thermal denaturation profiles of ctDNA (50 μM) in the absence and presence of VEM (50 μM). The inset shows the first derivative of the thermal denaturation curves, used for the precise determination of the melting temperature T_m . (d) Thermal denaturation profiles of ctDNA in the absence and presence of RhB (50 μM) and AO (50 μM), with arrows indicating the T_m values for each system. In panels (c,d), errors are within 2%. (e) Normalized absorbance ratio as a function of NaCl concentration for the ctDNA–VEM complex (PBS, pH = 7.4, 25 °C).

3.1.2. DNA Melting Study

The melting temperature (T_m) of DNA is a fundamental parameter that reflects the thermal stability of the double-stranded DNA helix. T_m is defined as the temperature at which 50% of the DNA in a sample transitions from the double-stranded to the single-stranded form, a process known as DNA denaturation [29]. This transition is typically monitored by

UV-vis spectroscopy, where the absorbance of DNA at 260 nm increases as the hydrogen bonds between the base pairs are disrupted, causing the DNA strands to separate [30,31]. The T_m provides critical insights into the stability of the DNA helix and can be influenced by various factors, including the presence of small molecules that bind to DNA.

Accordingly, the effect of VEM on the thermal stability of ctDNA was next investigated by measuring the T_m in the absence and presence of the drug. For comparison and validation purposes, measurements of T_m for ctDNA in the presence of Rhodamine B (RhB, a known DNA minor groove binder) or Acridine Orange (AO, a prototypical DNA intercalator) were also carried out. As seen in Figure 1c, the melting temperature of DNA alone was found to be 75.2 °C, which is consistent with the known properties of ctDNA under physiological ionic strength conditions [32]. This temperature reflects the inherent stability of the DNA helix, with hydrogen bonds and base-stacking interactions maintaining the double-stranded structure up to this point. When VEM was added to the DNA, the UV-vis spectra were recorded again as the temperature gradually increased. Notably, the melting temperature of the ctDNA was only slightly affected by the presence of VEM, with a determined T_m value of 77.1 °C (Figure 1c). Contextually, the same experiment performed in the presence of RhB yielded a T_m value close to that of pure ctDNA (78.2 °C), while the T_m value in the presence of AO was found to be substantially higher and equal to 81.5 °C (see Figure 1d). These observations are particularly telling about the nature of the interaction between VEM and DNA. In fact, typically small molecules that intercalate between the DNA base pairs significantly stabilize the DNA helix, leading to a marked increase (e.g., 5 to 8 °C or more) in the melting temperature [33], as in the present case of AO, for which a ΔT_m of 6.3 °C was recorded (Figure 1d). This is because intercalation enhances the π - π stacking interactions between the base pairs, thus making the DNA helix more resistant to thermal denaturation. However, molecules that bind to the minor groove of DNA often do not cause a significant shift in T_m [34], as seen here for RhB, for which a ΔT_m of only 3 °C was measured. This is because groove binding primarily involves interactions with the edges of the base pairs and the sugar-phosphate backbone, without significantly altering the overall helical structure or base stacking. The fact that VEM, like RhB, does not appreciably change the T_m of ctDNA indicates that it does not strongly stabilize or destabilize the DNA helix, consistent with a minor groove-binding mode.

3.1.3. Effect of Ionic Strength

The nature of the interaction between small molecules and DNA can be significantly influenced by the ionic strength of the surrounding environment. Electrostatic binding, which involves the attraction between positively charged molecules and the negatively charged phosphate backbone of DNA, is particularly sensitive to changes in ionic strength [35,36]. An increase in ionic strength typically screens these electrostatic interactions, reducing the binding affinity and resulting in observable changes in UV-vis absorbance. On the contrary, groove binding, which primarily involves hydrophobic interactions and hydrogen bonding within the minor or major grooves of the DNA helix, is much less affected by ionic strength [37].

To explore the possibility of electrostatic binding in the VEM-DNA assembly, UV-vis spectroscopy measurements were further performed at 260 nm for six DNA-VEM complexes, each in solutions of varying ionic strength. These experiments aimed to detect any changes in absorbance that could indicate a weakening of electrostatic interactions between the drug and the DNA. The results, however, revealed that the absorbance at 260 nm remained consistent at all ionic strength conditions, as illustrated in Figure 1e, supporting the idea that the main binding interaction between VEM and DNA is not electrostatic in nature and reinforcing the conclusion that it binds within the DNA groove rather than through electrostatic attraction to the DNA backbone.

3.2. Viscosity Studies

The viscosity of a nucleic acid solution is a crucial parameter that can be exploited to distinguish between intercalative binding and groove or electrostatic interactions. Intercala-

tive binding typically results in a significant increase in the viscosity of the solution, because the insertion of planar aromatic ligands between base pairs promotes their local separation, leading to a pronounced lengthening of the DNA helix. In contrast, groove binding and electrostatic interactions do not cause substantial changes in DNA length and therefore exhibit a minimal impact on viscosity [38,39]. To further elucidate the binding mechanism of VEM with ctDNA, the relative viscosity of the NA solution was evaluated at various concentrations of the drug, as shown in Figure 2a. For comparison purposes, the relative viscosity of ctDNA in the presence of RhB, a well-known groove-binding dye, and AO, a prototypical DNA intercalator [40], was measured. It was also assessed and is presented in the same figure. The data reveal that both VEM and RhB induced a similarly modest increase in the relative viscosity of the solutions, observed at all concentrations tested. On the contrary, in the presence of AO, the relative viscosity of ctDNA increased steadily, as expected. These findings indicate that VEM likely binds to ctDNA via a groove-binding mode, analogous to the interaction observed between AO and the nucleic acid.

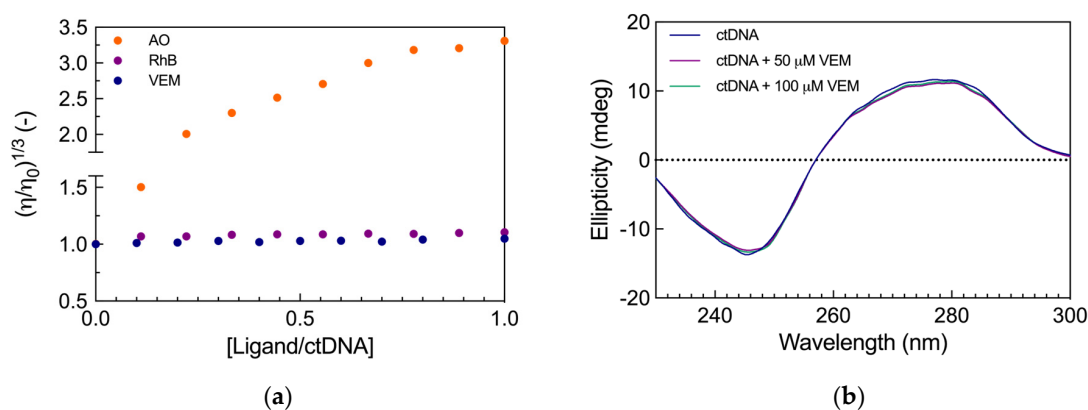


Figure 2. (a) Effect of increasing concentrations of VEM, RhB, and AO on the viscosity of ctDNA ([ctDNA] = 50 μ M, [ligand] = 0–50 μ M, PBS buffer, pH = 7.4, 25 $^{\circ}$ C). Each data point represents the mean of three independent measurements, with standard deviations smaller than the size of the data markers. (b) CD spectra of ctDNA recorded in the absence and presence of 50 μ M and 100 μ M of VEM in PBS buffer (pH 7.4, 25 $^{\circ}$ C).

3.3. CD Spectroscopy

Circular dichroism is a powerful and sensitive technique widely used to probe the conformational properties of nucleic acids, particularly DNA. This method is particularly effective in detecting even subtle changes in the secondary structure of DNA, such as transitions between different helical forms or distortions caused by ligand binding [41]. The CD spectrum of free ctDNA displayed the expected two prominent bands: a negative band at 243 nm, and a positive band at 277 nm (see Figure 2b). These spectral features are recognized as reliable markers indicative of the B-conformation of DNA and are sensitive to any perturbations induced by ligand binding [42]. Upon the addition of VEM at various concentrations, the CD spectra of ctDNA remained consistent, showing no significant changes in the intensity or position of these characteristic bands even at the highest concentrations of the drug used. The absence of spectral shifts in the presence of VEM supports the conclusion that the kinase inhibitor interacts with DNA through a groove-binding mode, a mechanism typically associated with minimal structural perturbation. This finding aligns with the earlier UV-vis spectroscopy results, which also indicated that VEM binding preserves the native B-conformation of the NA, further reinforcing the hypothesis that groove binding is the dominant interaction mode in this system.

3.4. Fluorescence Spectroscopy

Fluorescence spectroscopy is a versatile tool for studying interactions between small molecules and DNA [43]; however, both DNA and VEM are inherently weakly fluorescent.

This poses a challenge in the direct assessment of their interaction through fluorescence measurements. To overcome this limitation, competitive displacement assays were employed using AO again, known for its good affinity as a DNA intercalator, and RhB, which is a representative of minor groove binders [44]. When bound to DNA, these dyes exhibit a significant enhancement in fluorescence, making them excellent probes for studying displacement by other molecules. The basic principle of this assay is that, if VEM can displace any of such fluorescent dyes from DNA, it indicates that the drug binds to the DNA in a manner similar to that of the specific dye. This displacement would result in a measurable decrease in the fluorescence signal, providing indirect but clear evidence not only of the interaction between VEM and DNA, but also of the binding site mechanism (i.e., intercalation vs. groove binding). As shown in Figure 3a, the fluorescence spectrum of the DNA–RhB complex, with its peak emission at 576 nm, exhibited a pronounced decrease in intensity with the addition of VEM. This significant reduction in fluorescence is indicative of a competitive interaction, where the drug effectively displaces RhB from the minor groove of the DNA. However, the fluorescence spectrum of the DNA–AO complex, characterized by its peak emission at 525 nm, showed little variation even as the concentration of the drug increased (inset in Figure 3a). This subtle response suggests that VEM does not displace AO from its intercalative binding sites between the DNA base pairs, and therefore it does not interact with DNA through an intercalative mechanism. These observations, coupled with all other results from the experiments discussed above, provide substantial evidence that VEM primarily associates with DNA through groove binding.

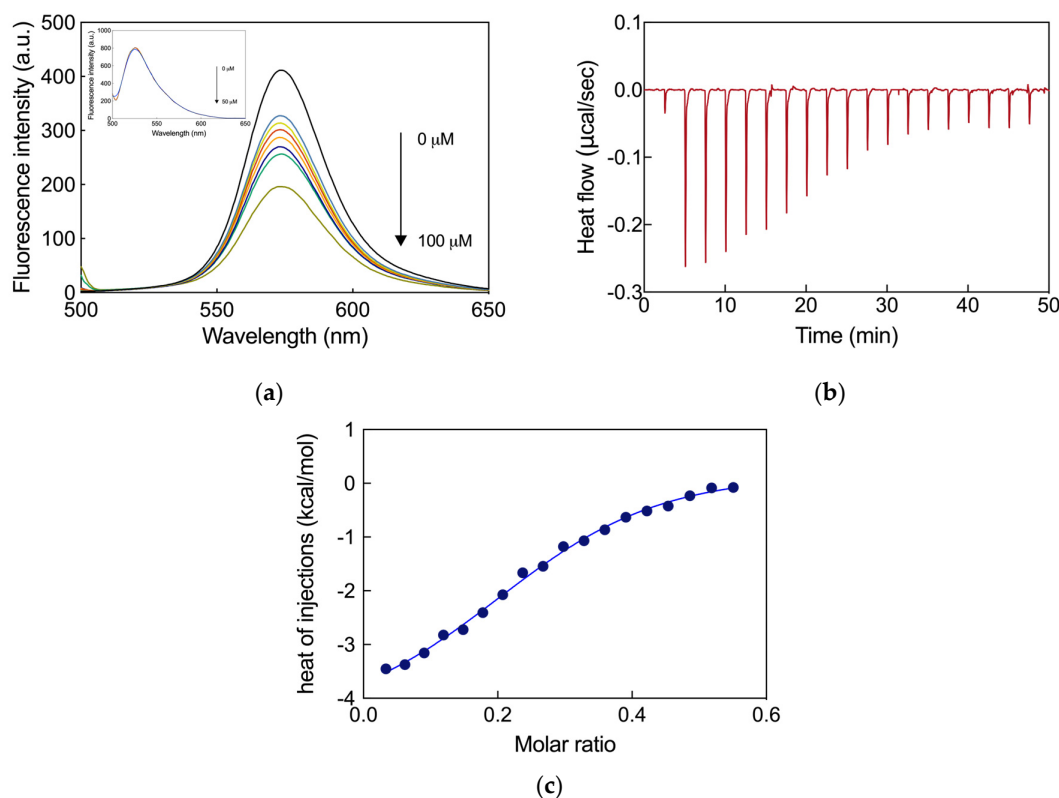


Figure 3. (a) Fluorescence spectra of the DNA–RhB complex in the presence of increasing concentrations of VEM (0 μM black, 2.5 μM cornflower blue, 5 μM dark khaki, 10 μM red, 15 μM orange, 20 μM blue, 50 μM green and 100 μM olive drab) (PBS buffer, pH = 7.4, 25 $^{\circ}\text{C}$). The inset shows the fluorescence spectra of the DNA–AO complex with increasing VEM concentrations (0 μM black, 2.5 μM blue, 5 μM cyan, 10 μM green, 20 μM orange, 50 μM red) under the same conditions. (b) ITC raw data and (c) the plot of the integrated ITC data for the interaction of ctDNA (40 μM , PBS buffer, pH = 7.4) and VEM at 25 $^{\circ}\text{C}$. The solid line corresponds to the data fitting with the one-site isothermal binding model.

3.5. Isothermal Titration Calorimetry

ITC is a robust and probe-free technique for directly assessing the thermodynamics of molecular interactions in solution [45–47]. It measures the heat changes associated with binding events, revealing essential thermodynamic parameters such as the variation of enthalpy (ΔH), entropy (ΔS), and Gibbs free energy (ΔG), and the related binding affinity K_d [48]. These parameters offer a comprehensive understanding of the binding process, including the forces driving the interaction and the stability of the resulting complex. In an ITC experiment, a titrant (typically a ligand or small molecule) is incrementally added to a solution containing the target molecule (such as a protein or nucleic acid). As the titrant binds to the target, heat is released or absorbed, depending on the nature of the interaction. This heat change is detected by the calorimeter and recorded as a function of time, generating a thermogram that can be analyzed to extract the thermodynamic parameters. One of the key advantages of ITC is its ability to provide a complete thermodynamic profile of an interaction in a single experiment, without the need for labeling or immobilization of the molecules. This makes it an invaluable tool for studying a wide range of biological processes (including, e.g., protein–ligand binding, DNA–drug interactions, and enzyme kinetics), thereby offering insights into the underlying molecular mechanisms.

Accordingly, ITC was used to quantitatively assess the thermodynamic parameters underlying the interaction between VEM and ctDNA. In this study, a fixed concentration of ctDNA was titrated with incremental aliquots of VEM, enabling a detailed analysis of the binding affinity, as well as the determination of the enthalpic and entropic contributions to the overall free energy change. The raw thermogram analysis shown in Figure 3b clearly shows that each discrete injection of VEM correlates with a negative heat flow peak, indicating that the interaction between the NA and the anticancer drug is exothermic. The sigmoidal shape of the integrated ITC data (Figure 3c), particularly the slope at the inflection point, enables the determination of the binding constant (K_d), which reflects a moderate affinity between ctDNA and VEM, with a mean value of 11.2 μM (Table 1). The corresponding variation in the change in free energy for the binding interaction (ΔG) was calculated as -6.76 kcal/mol, consistent with a spontaneous and thermodynamically favorable binding process. Further thermodynamic analysis of these data provided a comprehensive understanding of the interaction mechanisms characterizing the VEM–ctDNA interaction. The binding enthalpy change ΔH was determined to be -3.49 ± 0.34 kcal/mol, substantiating an exothermic interaction. This negative enthalpy suggests that the binding is driven by favorable interactions, such as hydrogen bonding and van der Waals forces, between VEM and the DNA. The change in entropy change ΔS , when multiplied by the temperature ($T\Delta S$), contributed 3.27 kcal/mol to the overall change in free energy. The positive value of $T\Delta S$ is suggestive of the presence of stabilizing hydrophobic contacts between the two binding partners and an increase in the disorder of the system upon binding, likely due to the release of water molecules or ions from the DNA groove as VEM binds. This, in turn, results in an overall increase in system entropy, which contributes favorably to the binding process. The estimated stoichiometry value (n) is 0.239, which is in line with what could be expected from a molecule of the size of VEM acting as a groove binder. Indeed, the reciprocal ($1/n$) could roughly represent the number of base pairs interacting with the ligand, and the resulting value (around 4) is reasonable.

ITC experiments were performed at four temperatures, ranging from 25 °C to 40 °C, to determine the molar heat capacity change (ΔC_p) associated with the binding process [49,50]. From the data shown in Table 1, it can be seen that, as the temperature increased, the negative contribution of ΔH became more pronounced, indicating favorable exothermic interaction, while the entropic contribution revealed an opposite trend. Both ΔH and ΔS exhibited a linear relationship with temperature, counterbalancing one another and thus resulting in an almost temperature-independent free energy variation for the binding interaction. This behavior, known as enthalpy–entropy compensation, suggests significant hydrophobic interactions during complex formation. The ΔC_p value was obtained from the first derivative of ΔH vs. temperature plot, yielding a ΔC_p of -172 cal/mol·°C (Table 1).

Consistent with prior observations [50–52], the negative sign of ΔC_p indicates the involvement of hydrophobic interactions, typically reflecting the burial of nonpolar surface areas upon complex formation. Moreover, the binding stoichiometry remained invariant across the temperature range, aligning with values calculated at 25 °C.

Table 1. ITC-derived thermodynamic parameters for the ctDNA–VEM complex at different temperatures. The errors in the listed values are within 10%.

T (°C)	K_d (μM)	n (–)	DH (kcal/mol)	–TDS (kcal/mol)	DG (kcal/mol)	DC_p (cal/mol °C)
25	11.2	0.239	–3.49	–3.27	–6.76	
30	11.8	0.258	–4.08	–2.76	–6.84	–172
37	10.7	0.241	–5.32	–1.74	–7.06	
40	10.3	0.223	–6.08	–1.07	–7.15	

3.6. Molecular Dynamics Simulations

Despite the extensive experimental validation of VEM binding to ctDNA reported above, the precise molecular details of this interaction remain elusive due to the absence of a crystal structure of the VEM–ctDNA complex. Under such circumstances, however, advanced computational methodologies can be aptly exploited to investigate and characterize the binding interactions at an atomic level. Traditional molecular dynamics (MD) simulations provide valuable insights but are often limited in their ability to capture the full complexity of drug–DNA interactions, particularly in systems with multiple potential binding sites and significant conformational flexibility. To address these challenges, the On-the-Fly Probability Enhanced Sampling with METADynamics-like target distribution (OPES-METAD) technique was employed in this work. Indeed, OPES-METAD allows for a comprehensive exploration of the free energy landscape (or free energy surface, FES) by applying a dynamic bias along selected collective variables (CVs) during the simulation. This enhanced sampling technique facilitates the identification of low-energy states corresponding to potential binding sites, enabling the system to traverse energy barriers that would otherwise be insurmountable in conventional MD simulations.

The first FES plot, shown in Figure 4a, illustrates the free energy landscape of the interaction between VEM and DNA as a function of the minimum distance from CG base pairs (dCG, x-axis) and AT base pairs (dAT, y-axis), with contour levels depicting the free energy levels (i.e., deeper-blue regions correspond to lower free energy states), indicating more favorable binding configurations for VEM. A distinct low-energy region is observed between 2 and 4 Å from the CG base pairs and 8 and 12 Å from the AT base pairs. This finding indicates that VEM has a stronger affinity for areas close to the CG base pairs, likely stabilized by direct interactions such as hydrogen bonding. The positioning of the energy minimum also implies that VEM may be bound within the minor groove of the DNA, where it can establish close contact with CG pairs. Although there is evidence of interaction with AT pairs, these interactions are less pronounced, as reflected by the shallower energy minimum associated with AT-rich regions. This observation implies that, while VEM does engage with AT pairs, its primary interactions occur with CG pairs, which likely play a more critical role in stabilizing the drug within the DNA groove. The second FES plot (Figure 4b) maps the free energy landscape as a function of the distance from the CG base pairs (dCG, x-axis) and the distance from the DNA edge (dEDGE, y-axis), with contour levels again depicting free energy values. The FES reveals a pronounced low-energy region between 2 and 4 Å from the CG base pairs and 8 and 12 Å from the DNA edge. This indicates that VEM exhibits a strong preference for binding to the central CG-rich regions within this sequence, specifically, the CG pairs located at positions 4–5 and 10–11. These CG pairs are flanked by AT-rich regions, yet the interactions of VEM with the CG bases appear to be more energetically favorable. The placement of the low-energy minimum at these distances suggests that VEM is positioned within the minor groove of the DNA, not

at the very edge, but deeper within the groove where it can form optimal contacts with the CG pairs. Overall, this FES analysis clearly identifies the central CG-rich regions of the DNA as the primary binding sites for VEM. The strong interaction with these CG pairs, located within the minor groove, allows for a stable, low-energy binding configuration.

In order to characterize in greater detail the binding mode and the underlying interactions between VEM and DNA, a configuration corresponding to the lowest free energy state in the FESs discussed above was extracted, and a further 4 μ s of unbiased MD simulations were carried out. The stability of the VEM–ctDNA complex was ensured by monitoring the root mean square displacement (RMSD) of VEM within the binding site, as shown in Figure 4c. While Figure 4d shows a snapshot isolated from the equilibrated portion of the 4 μ s unbiased MD simulation trajectory of the VEM–DNA complex, panel (e) in the same figure offers a zoomed view of the drug–NA binding mode, from which some of the main intermolecular interactions can be clearly observed. First, there is a permanent hydrogen bond (HB) between the H atom on the pyrrole nitrogen and the N3 atom of G4, characterized by an average dynamic length (ADL) of 2.76 ± 0.2 Å with a lifetime (LT), expressed as the percentage of the total simulation time (5 μ s), 78.0%, and a second HB involving the amino group (NH_2) of the same nucleotide and the N atom in the pyridine ring of the drug (ADL = 2.43 ± 0.3 Å, LT = 75.7%). Interestingly, the MD simulation also revealed the presence of two molecules of water bridging the NA and the drug via HBs. As seen again in Figure 4d, the first water molecule donates two HBs (LT = 68.6%), the first involving the G4 phosphate group (ADL = 1.82 ± 0.2 Å), and the latter engaging the drug sulfonyl group (ADL = 1.85 ± 0.2 Å). The second water molecule (LT = 71.5%) accepts an HB from the sulfonamide HN- moiety (1.95 ± 0.1 Å) while donating two HBs involving the carbonyl group ($-\text{C}=\text{O}$) of C5 on one strand (1.94 ± 0.2 Å) and the same moiety of T6 in the opposite strand (1.73 ± 0.1 Å). These interactions, along with the network of favorable van der Waals, polar, and hydrophobic contacts between VEM and DNA within the binding region, account and explain the affinity of VEM for the DNA minor groove, and provide a molecular-based rationale for the experimental value of the drug–NA affinity measured by ITC.

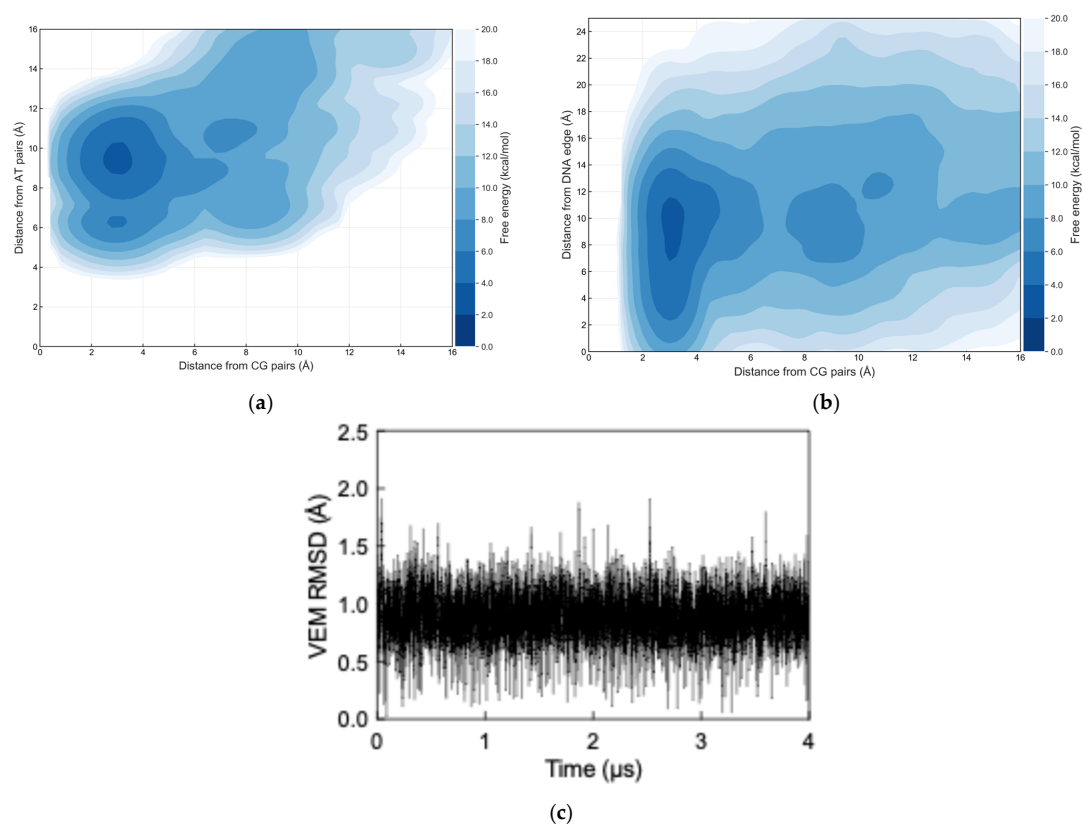


Figure 4. Cont.

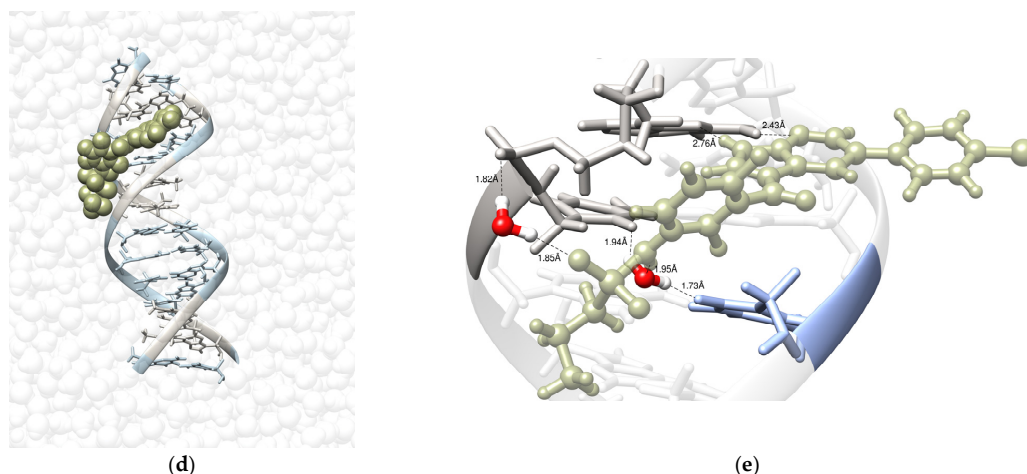


Figure 4. Free energy surface (FES) as obtained from OPES-METAD simulations for the interaction between VEM and DNA (a) as a function of the minimum distance from CG base pairs (dCG) and AT base pairs (dAT), and (b) as a function of the distance function of the distance dCG and the distance from the DNA edge (dEDGE). (c) Root mean square displacement (RMSD) of VEM over time in the unbiased simulation. (d) Snapshot extracted from the equilibrated portion of the 4 μ s unbiased MD simulation trajectory of the VEM–DNA complex. The DNA bases are shown in sticks and balls and colored as follows: adenines and thymines, winter sky; guanines and cytosines, moonstruck gray. VEM is portrayed in fern-colored spheres, while surrounding water molecules are depicted in transparent lucent white. Ions and counterions are not shown for clarity. (e) Main interactions involved in the DNA minor groove binding by VEM as obtained from the relevant equilibrated portion of the corresponding 4 μ s unbiased MD simulation trajectory. The water molecules involved in hydrogen bonds with the NA and the drug are shown in atom-colored sticks and balls (O, red; H, white). All other water molecules, ions, and counterions are not shown for clarity.

4. Conclusions

This work provides a comprehensive and multifaceted understanding of the interactions between Vemurafenib and calf thymus DNA, revealing critical insights that go beyond its primary mechanism of action as a BRAF inhibitor. Through the use of advanced biophysical techniques and molecular dynamics simulations, it has been demonstrated that VEM binds to DNA through a non-intercalative, groove-binding mechanism, specifically interacting with CG-rich regions in the DNA minor groove. This binding mode is essential as it ensures minimal disruption to the structural integrity of the DNA helix, which is a significant finding given the concerns around potential genotoxicity associated with small-molecule therapeutics like VEM.

The experimental data, including UV-vis absorption spectroscopy, circular dichroism, and fluorescence spectroscopy, consistently support the conclusion that VEM does not induce significant structural changes in DNA. This contrasts with intercalative agents, which often cause substantial perturbations to the DNA double helix, leading to genomic instability. The slight changes observed in the thermal denaturation studies further reinforce the notion that the interaction of VEM with DNA is relatively benign in terms of structural impact, thus reducing the risk of inducing DNA damage or interfering with essential biological processes like replication and transcription.

The thermodynamic parameters obtained from isothermal titration calorimetry provide further depth to this understanding. The exothermic nature of the interaction, characterized by favorable enthalpy and entropy changes, highlights the importance of hydrogen bonding, van der Waals interactions, and hydrophobic contacts in stabilizing the VEM–DNA complex. The release of water molecules during binding, as indicated by the positive entropy contribution, suggests that VEM binding leads to an increase in system disorder, a hallmark of groove-binding interactions where the ligand displaces water molecules from the DNA surface without causing major conformational changes.

Molecular dynamics simulations complement these findings by offering atomic-level insights into the binding process. The simulations reveal that VEM exhibits a strong preference for CG-rich regions in the minor groove, forming stable hydrogen bonds with the DNA bases. This binding configuration is further stabilized by water molecules that bridge between VEM and DNA, forming a network of interactions that enhance the ligand affinity without compromising the structural integrity of the DNA. The computational results corroborate the experimental data, providing a detailed map of the binding interactions and offering a robust framework for understanding how VEM interacts with DNA at the molecular level.

These findings have significant implications for the clinical use of VEM, particularly in long-term treatments where cumulative off-target effects could pose a risk to patients. The fact that VEM binds to DNA in a manner that avoids major structural disruptions suggests that its potential for causing genotoxic side effects may be lower than previously anticipated. However, this does not eliminate the need for continued vigilance in monitoring its long-term effects, especially in the context of its prolonged use in cancer therapies. Understanding these interactions at a molecular level is critical for optimizing the therapeutic profile of VEM and ensuring that its benefits in treating melanoma and other cancers outweigh any potential risks.

In conclusion, this study not only enhances the molecular understanding of VEM–DNA interactions but also underscores the importance of using a combination of experimental and computational techniques to fully characterize drug–DNA interactions. The insights gained from this research will be valuable not only for optimizing the clinical use of VEM but also for guiding the design of future drugs that target DNA or have the potential to interact with genomic material. By elucidating the precise nature of VEM–DNA binding, this study lays the groundwork for more informed decisions in drug design and therapy optimization, ultimately contributing to safer and more effective treatments for patients.

Author Contributions: Conceptualization, E.L. and S.P.; methodology, G.C., E.L., D.M. and S.P.; software, D.M.; formal analysis, G.C., R.P., D.M., E.L. and S.P.; investigation, G.C., R.P. and D.M.; data curation, G.C., R.P. and D.M.; writing—original draft preparation, G.C., R.P., D.M., E.L. and S.P.; writing—review and editing, S.P.; supervision, E.L. and S.P.; project administration, E.L. and S.P.; funding acquisition, E.L. and S.P. All authors have read and agreed to the published version of the manuscript.

Funding: This research was funded by ICSC-Centro Nazionale di Ricerca in high-performance computing, big data, and quantum computing (Spoke 7, WP4 (Pilot applications), and T.2.8 (“Development and optimization of HPC-based integrated workflows based on flagship codes for personalized (nano)medicine”) to E.L. and S.P.). The authors wish also to acknowledge the generous financial support from the Italian Association for Cancer Research (AIRC, grant for “Novel hot-spot mutations in BCR-ABL1: role in resistance to CML target therapy–IG17413” to S.P.) and the Fondazione Cassa di Risparmio di Trieste (Fondazione CRTrieste, grant for “Far-UV CD spectroscopy in translational medicine” to S.P.).

Institutional Review Board Statement: Not applicable.

Informed Consent Statement: Not applicable.

Data Availability Statement: The original contributions presented in the study are included in the article. Further inquiries can be directed to the corresponding author.

Acknowledgments: Authors wish to acknowledge the CINECA award (proposal DoCry, HP10C5SVI2) under the ISCRA initiative for the availability of high-performance computing resources and support.

Conflicts of Interest: The authors declare no conflicts of interest.

References

1. Watanabe, K.; Seki, N. Biology and Development of DNA-Targeted Drugs, Focusing on Synthetic Lethality, DNA Repair, and Epigenetic Modifications for Cancer: A Review. *Int. J. Mol. Sci.* **2024**, *25*, 752. [[CrossRef](#)] [[PubMed](#)]
2. Childs-Disney, J.L.; Yang, X.; Gibaut, Q.M.R.; Tong, Y.; Batey, R.T.; Disney, M.D. Targeting RNA structures with small molecules. *Nat. Rev. Drug Discov.* **2022**, *21*, 736–762. [[CrossRef](#)] [[PubMed](#)]
3. Khan, H.Y.; Ansari, M.F.; Tabassum, S.; Arjmand, F. A review on the recent advances of interaction studies of anticancer metal-based drugs with therapeutic targets, DNA and RNAs. *Drug Discov. Today* **2024**, *29*, 104055. [[CrossRef](#)] [[PubMed](#)]
4. Wang, M.; Yu, Y.; Liang, C.; Lu, A.; Zhang, G. Recent Advances in Developing Small Molecules Targeting Nucleic Acid. *Int. J. Mol. Sci.* **2016**, *17*, 779. [[CrossRef](#)]
5. Rescifina, A.; Zagni, C.; Varrica, M.G.; Pistara, V.; Corsaro, A. Recent advances in small organic molecules as DNA intercalating agents: Synthesis, activity, and modeling. *Eur. J. Med. Chem.* **2014**, *74*, 95–115. [[CrossRef](#)] [[PubMed](#)]
6. Groelly, F.J.; Fawkes, M.; Dagg, R.A.; Blackford, A.N.; Tarsounas, M. Targeting DNA damage response pathways in cancer. *Nat. Rev. Cancer* **2023**, *23*, 78–94. [[CrossRef](#)]
7. Gu, L.; Hickey, R.J.; Malkas, L.H. Therapeutic Targeting of DNA Replication Stress in Cancer. *Genes* **2023**, *14*, 1346. [[CrossRef](#)]
8. Zhu, W.; Wang, Y.; Li, K.; Gao, J.; Huang, C.H.; Chen, C.C.; Ko, T.P.; Zhang, Y.; Guo, R.T.; Oldfield, E. Antibacterial drug leads: DNA and enzyme multitargeting. *J. Med. Chem.* **2015**, *58*, 1215–1227. [[CrossRef](#)]
9. Butler, M.S.; Vollmer, W.; Goodall, E.C.A.; Capon, R.J.; Henderson, I.R.; Blaskovich, M.A.T. A Review of Antibacterial Candidates with New Modes of Action. *ACS Infect. Dis.* **2024**, *10*, 3440–3474. [[CrossRef](#)] [[PubMed](#)]
10. Bollag, G.; Tsai, J.; Zhang, J.; Zhang, C.; Ibrahim, P.; Nolop, K.; Hirth, P. Vemurafenib: The first drug approved for BRAF-mutant cancer. *Nat. Rev. Drug Discov.* **2012**, *11*, 873–886. [[CrossRef](#)]
11. Castellani, G.; Buccarelli, M.; Arasi, M.B.; Rossi, S.; Pisanu, M.E.; Bellenghi, M.; Lintas, C.; Tabolacci, C. BRAF Mutations in Melanoma: Biological Aspects, Therapeutic Implications, and Circulating Biomarkers. *Cancers* **2023**, *15*, 4026. [[CrossRef](#)] [[PubMed](#)]
12. Vargiu, A.V.; Ruggerone, P.; Magistrato, A.; Carloni, P. Dissociation of minor groove binders from DNA: Insights from metadynamics simulations. *Nucleic Acids Res.* **2008**, *36*, 5910–5921. [[CrossRef](#)] [[PubMed](#)]
13. Galindo-Murillo, R.; Robertson, J.C.; Zgarbová, M.; Šponer, J.; Otyepka, M.; Jurečka, P.; Cheatham, T.E. Assessing the Current State of Amber Force Field Modifications for DNA. *J. Chem. Theory Comput.* **2016**, *12*, 4114–4127. [[CrossRef](#)] [[PubMed](#)]
14. Russi, M.; Cavalieri, G.; Marson, D.; Laurini, E.; Pricl, S. Binding of the B-Raf Inhibitors Dabrafenib and Vemurafenib to Human Serum Albumin: A Biophysical and Molecular Simulation Study. *Mol. Pharm.* **2022**, *19*, 1619–1634. [[CrossRef](#)]
15. Junmei, W.; Romain, M.W.; James, W.C.; Peter, A.K.; David, A.C. Development and testing of a general amber force field. *J. Comput. Chem.* **2004**, *25*, 1157–1174. [[CrossRef](#)]
16. Vanqualef, E.; Simon, S.; Marquant, G.; Garcia, E.; Klimerak, G.; Delepine, J.C.; Cieplak, P.; Dupradeau, F.-Y. R.E.D. Server: A web service for deriving RESP and ESP charges and building force field libraries for new molecules and molecular fragments. *Nucleic Acids Res.* **2011**, *39*, W511–W517. [[CrossRef](#)]
17. Invernizzi, M.; Parrinello, M. Rethinking Metadynamics: From Bias Potentials to Probability Distributions. *J. Phys. Chem. Lett.* **2020**, *11*, 2731–2736. [[CrossRef](#)]
18. Tribello, G.A.; Bonomi, M.; Branduardi, D.; Camilloni, C.; Bussi, G. PLUMED 2: New feathers for an old bird. *Comput. Phys. Commun.* **2014**, *185*, 604–613. [[CrossRef](#)]
19. Loncharich, R.J.; Brooks, B.R.; Pastor, R.W. Langevin dynamics of peptides: The frictional dependence of isomerization rates of N-acetylalanine-N'-methylamide. *Biopolymers* **1992**, *32*, 523–535. [[CrossRef](#)]
20. Berendsen, H.J.C.; Postma, J.P.M.; van Gunsteren, W.F.; DiNola, A.; Haak, J.R. Molecular dynamics with coupling to an external bath. *J. Chem. Phys.* **1984**, *81*, 3684–3690. [[CrossRef](#)]
21. Gomez, Y.K.; Natale, A.M.; Lincoff, J.; Wolgemuth, C.W.; Rosenberg, J.M.; Grabe, M. Taking the Monte-Carlo gamble: How not to buckle under the pressure! *J. Comput. Chem.* **2022**, *43*, 431–434. [[CrossRef](#)] [[PubMed](#)]
22. Ryckaert, J.-P.; Ciccotti, G.; Berendsen, H.J.C. Numerical integration of the cartesian equations of motion of a system with constraints: Molecular dynamics of n-alkanes. *J. Comput. Phys.* **1977**, *23*, 327–341. [[CrossRef](#)]
23. Hopkins, C.W.; Le Grand, S.; Walker, R.C.; Roitberg, A.E. Long-Time-Step Molecular Dynamics through Hydrogen Mass Repartitioning. *J. Chem. Theory Comput.* **2015**, *11*, 1864–1874. [[CrossRef](#)]
24. Toukmaji, A.; Sagui, C.; Board, J.; Darden, T. Efficient particle-mesh Ewald based approach to fixed and induced dipolar interactions. *J. Chem. Phys.* **2000**, *113*, 10913–10927. [[CrossRef](#)]
25. Case, D.A.; Aktulga, H.M.; Belfon, K.; Ben-Shalom, I.Y.; Berryman, J.T.; Brozell, S.R.; Cerutti, D.S.; Cheatham, T.E., III; Cisneros, G.A.; Cruzeiro, V.W.D.; et al. *AMBER 2022*; University of California: San Francisco, CA, USA, 2022.
26. Abraham, M.J.; Murtola, T.; Schulz, R.; Páll, S.; Smith, J.C.; Hess, B.; Lindahl, E. GROMACS: High performance molecular simulations through multi-level parallelism from laptops to supercomputers. *Software* **2015**, *1–2*, 19–25. [[CrossRef](#)]
27. Takahashi, H.; Nishikawa, S. Spectroscopic Studies of Nucleic Acids. In *Nucleic Acids in Chemistry and Biology*; Blackburn, G.M., Gait, M.J., Loakes, D., Williams, D.M., Eds.; Royal Society of Chemistry: London, UK, 2015; pp. 301–338.
28. Sirajuddin, M.; Ali, S.; Badshah, A. Drug-DNA interactions and their study by UV-Visible, fluorescence spectroscopies and cyclic voltametry. *J. Photochem. Photobiol. B* **2013**, *124*, 1–19. [[CrossRef](#)]

29. Wartell, R.M.; Benight, A.S. Thermal denaturation of DNA molecules: A comparison of theory with experiment. *Phys. Rep.* **1985**, *126*, 67–107. [[CrossRef](#)]
30. Tataurov, A.V.; You, Y.; Owczarzy, R. Predicting ultraviolet spectrum of single stranded and double stranded deoxyribonucleic acids. *Biophys. Chem.* **2008**, *133*, 66–70. [[CrossRef](#)]
31. Lando, D.Y.; Fridman, A.S.; Chang, C.-L.; Grigoryan, I.E.; Galyuk, E.N.; Murashko, O.N.; Chen, C.-C.; Hu, C.-K. Determination of melting temperature and temperature melting range for DNA with multi-peak differential melting curves. *Anal. Biochem.* **2015**, *479*, 28–36. [[CrossRef](#)]
32. Khandelwal, G.; Bhyravabhotla, J. A phenomenological model for predicting melting temperatures of DNA sequences. *PLoS ONE* **2010**, *5*, e12433. [[CrossRef](#)]
33. Almaqwashi, A.A.; Paramanathan, T.; Rouzina, I.; Williams, M.C. Mechanisms of small molecule–DNA interactions probed by single-molecule force spectroscopy. *Nucleic Acids Res.* **2016**, *44*, 3971–3988. [[CrossRef](#)] [[PubMed](#)]
34. Zhang, X.-X.; Brantley, S.L.; Corcelli, S.A.; Tokmakoff, A. DNA minor-groove binder Hoechst 33258 destabilizes base-pairing adjacent to its binding site. *Commun. Biol.* **2020**, *3*, 525. [[CrossRef](#)] [[PubMed](#)]
35. Sha, Y.; Chen, X.; Niu, B.; Chen, Q. The Interaction Mode of Groove Binding between Quercetin and Calf Thymus DNA Based on Spectrometry and Simulation. *Chem. Biodivers.* **2017**, *14*, e1700133. [[CrossRef](#)] [[PubMed](#)]
36. Pan, B.; Lv, M.; Du, H.; Zhao, D.; Lu, K. Spectroscopic studies on noncovalent binding of nicotinamide–modified BRCA1 (856–871) analogs to calf thymus DNA. *Spectrochim. Acta Part A Mol. Biomol. Spectrosc.* **2023**, *294*, 122531. [[CrossRef](#)] [[PubMed](#)]
37. Amado, A.M.; Pazin, W.M.; Ito, A.S.; Kuzmin, V.A.; Borissevitch, I.E. Acridine orange interaction with DNA: Effect of ionic strength. *Biochim. Biophys. Acta Gen. Subj.* **2017**, *1861*, 900–909. [[CrossRef](#)]
38. Shi, J.-H.; Chen, J.; Wang, J.; Zhu, Y.-Y. Binding interaction between sorafenib and calf thymus DNA: Spectroscopic methodology, viscosity measurement and molecular docking. *Spectrochim. Acta Part A Mol. Biomol. Spectrosc.* **2015**, *136*, 443–450. [[CrossRef](#)]
39. Phadte, A.A.; Banerjee, S.; Mate, N.A.; Banerjee, A. Spectroscopic and viscometric determination of DNA-binding modes of some bioactive dibenzodioxins and phenazines. *Biochem. Biophys. Rep.* **2019**, *18*, 100629. [[CrossRef](#)]
40. Bi, S.; Qiao, C.; Song, D.; Tian, Y.; Gao, D.; Sun, Y.; Zhang, H. Study of interactions of flavonoids with DNA using acridine orange as a fluorescence probe. *Sens. Actuators B Chem.* **2006**, *119*, 199–208. [[CrossRef](#)]
41. Chang, Y.M.; Chen, C.K.; Hou, M.H. Conformational changes in DNA upon ligand binding monitored by circular dichroism. *Int. J. Mol. Sci.* **2012**, *13*, 3394–3413. [[CrossRef](#)]
42. Miyahara, T.; Nakatsuji, H.; Sugiyama, H. Helical Structure and Circular Dichroism Spectra of DNA: A Theoretical Study. *J. Phys. Chem. A* **2013**, *117*, 42–55. [[CrossRef](#)]
43. Luikham, S.; Mavani, A.; Sinha, D.; Bhattacharyya, J. Structural Insight into Groove Binding of Yohimbine with Calf Thymus DNA: A Spectroscopic, Calorimetric, and Computational Approach. *J. Phys. Chem. B* **2023**, *127*, 4966–4978. [[CrossRef](#)] [[PubMed](#)]
44. Husain, M.A.; Ishqi, H.M.; Rehman, S.U.; Sarwar, T.; Afrin, S.; Rahman, Y.; Tabish, M. Elucidating the interaction of sulindac with calf thymus DNA: Biophysical and in silico molecular modelling approach. *New J. Chem.* **2017**, *41*, 14924–14935. [[CrossRef](#)]
45. Saboury, A.A. A review on the ligand binding studies by isothermal titration calorimetry. *J. Iran. Chem. Soc.* **2006**, *3*, 1–21. [[CrossRef](#)]
46. Su, H.; Xu, Y. Application of ITC-Based Characterization of Thermodynamic and Kinetic Association of Ligands with Proteins in Drug Design. *Front. Pharmacol.* **2018**, *9*, 1133. [[CrossRef](#)]
47. Laurini, E.; Aulic, S.; Skoko, N.; Marson, D.; Fermeglia, M.; Pricl, S. ITC for Characterization of Self-Assembly Process of Cationic Dendrons for siRNA Delivery. *Methods Mol. Biol.* **2021**, *2282*, 245–266. [[CrossRef](#)] [[PubMed](#)]
48. Dhal, A.; Nayim, S.; Pattanayek, S.; Khatun, M.; Barman, S.; Paria, S.; Shit, B.; Kundu, S.; Jha, P.K.; Hossain, M. Evaluation of calf thymus DNA binding of newly synthesized five 9 O Imidazolyl alkyl berberine derivative: A comparative multi-spectroscopic and calorimetric study. *Int. J. Biol. Macromol.* **2023**, *253*, 126958. [[CrossRef](#)]
49. Chaires, J.B. Energetics of drug–DNA interactions. *Biopolymers* **1997**, *44*, 201–215. [[CrossRef](#)]
50. Bhadra, K.; Kumar, G.S. Isoquinoline alkaloids and their binding with DNA: Calorimetry and thermal analysis applications. *Mini Rev. Med. Chem.* **2010**, *10*, 1235–1247. [[CrossRef](#)]
51. Basu, A.; Suresh Kumar, G. Studies on the interaction of the food colorant tartrazine with double stranded deoxyribonucleic acid. *J. Biomol. Struct. Dyn.* **2015**, *34*, 935–942. [[CrossRef](#)]
52. Das, A.; Suresh Kumar, G.; Dutta, S. Interaction of aloe active compounds with calf thymus DNA. *J. Mol. Recognit.* **2019**, *32*, e2786. [[CrossRef](#)]

Disclaimer/Publisher’s Note: The statements, opinions and data contained in all publications are solely those of the individual author(s) and contributor(s) and not of MDPI and/or the editor(s). MDPI and/or the editor(s) disclaim responsibility for any injury to people or property resulting from any ideas, methods, instructions or products referred to in the content.